IOP Conf. Series: Materials Science and Engineering **297** (2018) 012032 doi:10.1088/1757-899X/297/1/012032

The evolution of homogeneous isotropic turbulence in background rotation

Jiratrakul Tunkeaw and Watchapon Rojanaratanangkule*

Faculty of Engineering, Department of Mechanical Engineering, Chiang Mai University, Chiang Mai 50200, Thailand

*Corresponding Author: watchapon.roj@eng.cmu.ac.th

Abstract. Direct numerical simulation is employed to investigate the effect of background rotation on the evolution of homogeneous isotropic turbulence. The frame of reference rotates only in one direction with a rotation numbers varied from 0 to 4, representing both slow and fast rotations. In a stationary frame of reference, the turbulence structures are isotropic and its energy spectrum exhibits a famous $\kappa^{-5/3}$ in the inertial subrange. The background rotation alters the isotropic behaviour of the turbulence structures, leading to the formation of columnar vortices. The slope of the energy spectrum strongly depends on the rotation number and ranges between -5/3 and -3.78.

1. Introduction

Turbulence in background rotation is a fascinating problem because of its appearance in a broad variety of geophysical, astrophysical and engineering applications (e.g. turbomachinery, planetary rotation, etc.). Experiments of grid-generated decaying turbulence in a rotating tank reveals that the slope of energy spectrum $E(\kappa)$ exhibits a rotation number dependent ranging between -5/3 (slow rotation) and about -2.3 (fast rotation) [1]. Early numerical simulations of decaying isotropic turbulence in background rotation observed the reduction in the energy flux and the two-dimensionalisation of the flow [2–4]. However, the conclusive results on the spectral properties of turbulence were still missing because only turbulence at low Reynolds numbers could be considered at that time due to the limitation of the computational resources. Godeferd & Lollini [5] and Morinishi *et al.* [6] performed direct numerical simulation (DNS) at higher Reynolds numbers and observed the similar behaviour of the correlation lengths and the decay properties of the kinetic turbulent energy as those found in the experiments of Hopfinger *et al.* For isotropic turbulence with large scale forcing, the energy spectrum behaves as κ^{-2} in the inertial subrange [8, 9]. In contrast, once the turbulence is forced at intermediate scales, the double cascade was found [9, 10]. The energy spectrum exhibits an inverse cascade with a slope of κ^{-3} scaling in a region of wavenumbers $\kappa < \kappa_{\text{forcing}}$ [9, 10], together with κ^{-2} behaviour when $\kappa > \kappa_{\text{forcing}}$ [10–11]. Baqui & Davidson [12] predicted that the growth in anisotropy increases linearly as $l_{\parallel}/l_{\perp} \sim \Omega t$ (where $l_{\perp}$ and $l_{\parallel}$ respectively being the integral scale in the direction perpendicular and parallel to the rotation axis). Furthermore, they showed that the rate of dissipation of energy changes as $\varepsilon \sim u^3/l_{\perp}$ in the inertial range for turbulence in a rotating background. Large eddy simulations were also used to investigate the effects of background rotation

on homogeneous isotropic turbulence (HIT) by Yang & Domaradzki [13]. They found that at high Reynolds numbers, the energy spectrum exhibits a κ^{-2} slope for the quasi-isotropic state, while a κ^{-3} spectrum forms for a strongly anisotropic state. Additionally, the Reynolds stress tensor becomes anisotropic after long enough time for low rotation rates but returns to an isotropic state for very strong rotation rates.

The aim of this work is to investigate the response of isotropic turbulence under uniform background rotation in a vertical direction to explore the evolution of the turbulence structures and the dynamic of the energy spectrum.

2. Numerical Approach

The flow considered in this work is governed by the incompressible continuity and Navier–Stokes equations written in a Cartesian tensor notation as

$$\frac{\partial u_i}{\partial x_i} = 0 \tag{1}$$

$$\frac{\partial u_i}{\partial t} - \varepsilon_{ijk} u_j \omega_k = -\frac{1}{\rho}\frac{\partial P_{eff}}{\partial x_i} + \nu \frac{\partial^2 u_i}{\partial x_j \partial x_j} + +2\varepsilon_{ijk} u_j \Omega_k \tag{2}$$

where $x_i = (x, y, z)$ and $u_i = (u, v, w)$ are respectively Cartesian coordinates and the corresponding velocity vector, $\omega_i = \varepsilon_{ijk}\partial u_k / \partial x_j$ is the vorticity vector and ε_{ijk} is the Levi–Civita symbol. The quantity t denotes time and the effective pressure $P_{eff} = p + \rho u_j u_j / 2$ includes the thermodynamics pressure p and the kinetic energy (the summation over the subscript j being implied). The fluid properties, which are density ρ and kinematic viscosity ν, are assumed constant. The frame of reference is rotated in the vertical direction with a constant angular velocity $\Omega_i = (0, 0, \Omega_z)$.

The simulations are conducted in a periodic cubic box of length $2\pi \times 2\pi \times 2\pi$. It is thus suitable to Fourier transform the governing equations to perform the spatial derivative. The viscous term is integrated analytically using an integrating-factor approach [14]. The Fourier-transformed Navier–Stokes equations reduce to

$$\frac{\partial}{\partial t}\left(I_v \hat{u}_i\right) = I_v\left(-\hat{i}\kappa_i P_{\text{eff}} + \hat{H}_i\right) \tag{3}$$

where $\hat{u}_i = (\hat{u}, \hat{v}, \hat{w})$ is the velocity in the Fourier space, $I_v = \exp\left[\nu \kappa_j \kappa_j t\right]$ is the integrating factor, $\kappa_i = (\kappa_x, \kappa_y, \kappa_z)$ is the wavenumber in each direction of the Cartesian coordinates, $\hat{i} = \sqrt{-1}$ and $\hat{H}_m$ is the nonlinear term. Equation (3) is advanced in time with a low-storage third-order Runge–Kutta scheme [15]. The divergence-free constrain is enforced via a standard pressure-projection method. The nonlinear and Coriolis terms $\varepsilon_{ijk} u_j \left(\omega_k + 2\Omega_k\right)$ are computed in a real space and then dealiased using the 3/2-rule in the Fourier space.

The initial condition is obtained from the preliminary simulation, whose initial spectrum is given as

$$E(\kappa, 0) = \frac{q^2 \kappa^\sigma}{2A\kappa_p^{\sigma+1}} \exp\left[-\frac{\sigma}{2}\left(\frac{\kappa}{\kappa_p}\right)^2\right] \tag{4}$$

where $\sigma = 2$ is a free parameter, $\kappa_p = 13$ is the peak location of the spectrum, $q^2 = 3$ is twice the initial kinetic energy, $\kappa = (\kappa_j \kappa_j)^{1/2}$ is the wavenumber magnitude and

$$A = \int_0^\infty \frac{\kappa^\sigma}{\kappa_p^{\sigma+1}} \exp\left[-\frac{\sigma}{2}\left(\frac{\kappa}{\kappa_p} \right)^2 \right] \mathrm{d}\kappa \ . \tag{5}$$

The preliminary simulation was performed with the resolution of $160\times160\times160$ and was advanced until $t = 6$, at which the realistic HIT develops. It should be noted that the grid used throughout this work is uniform. It can be seen from figure 1 that the energy spectrum at this time is in very good agreement with that of Orlandi [16] and Mansour & Wray [17] at almost the same Taylor-scale Reynolds number $R_\lambda = \left(u'u'\right)^{1/2} \lambda / \nu$ (where λ and u' respectively being the Taylor's microscale and the fluctuation velocity).

To investigate the effect of the background rotation, the rotation number $N = 2\Omega_z L_z / 2\pi u_0'$ (where L_z being the length of the computational domain in the vertical direction and u_0' being the initial fluctuating velocity) is varied from 0 to 4.

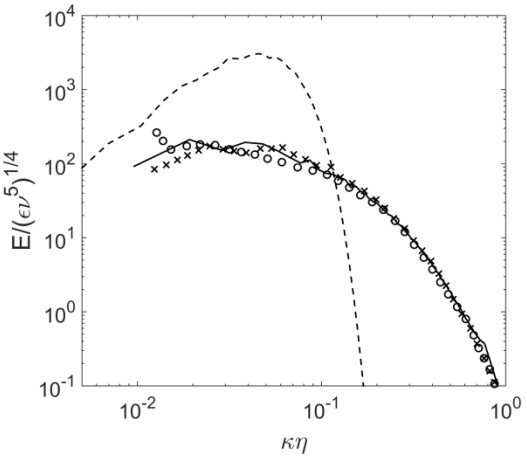

Figure 1. Energy spectra normalized by Kolmogorov units at; - - - - initial spectrum, ----- present simulation ($Re_\lambda = 55.8$), × Orlandi ($Re_\lambda = 54.3$) [16] and ○ Mansour & Wray ($Re_\lambda = 54.1$) [17].

3. Results

3.1. *Flow Visualizations*

The structure of the three-dimensional turbulence with and without the effect of external rotation is visualised by means of the isosurfaces of the second invariant of the velocity gradient tensor $Q = -0.5 u_{i,j} u_{j,i}$, normalised by $\omega_0^2 / 4$ (where ω_0 being the magnitude of the initial vorticity). The non-dimensional time is defined as $t^* = t\varepsilon_0 / ke_0$ (where the initial dissipation rate and kinetic energy are respectively denoted by ε_0 and ke_0).

Figures 2(a), 2(c) and 2(e) respectively show the evolution of the turbulence structures at $N = 0,\ 0.25$ and 0.5 at $t^* = 1.7$. At this time, the turbulence structures for these three cases develop in the same manner and look isotropic. The Taylor's length scale at this time is almost equal at about $\lambda \approx 0.15$. In contrast, at $t^* = 8.5$, the Taylor's length scale increases with an increase in the rotation

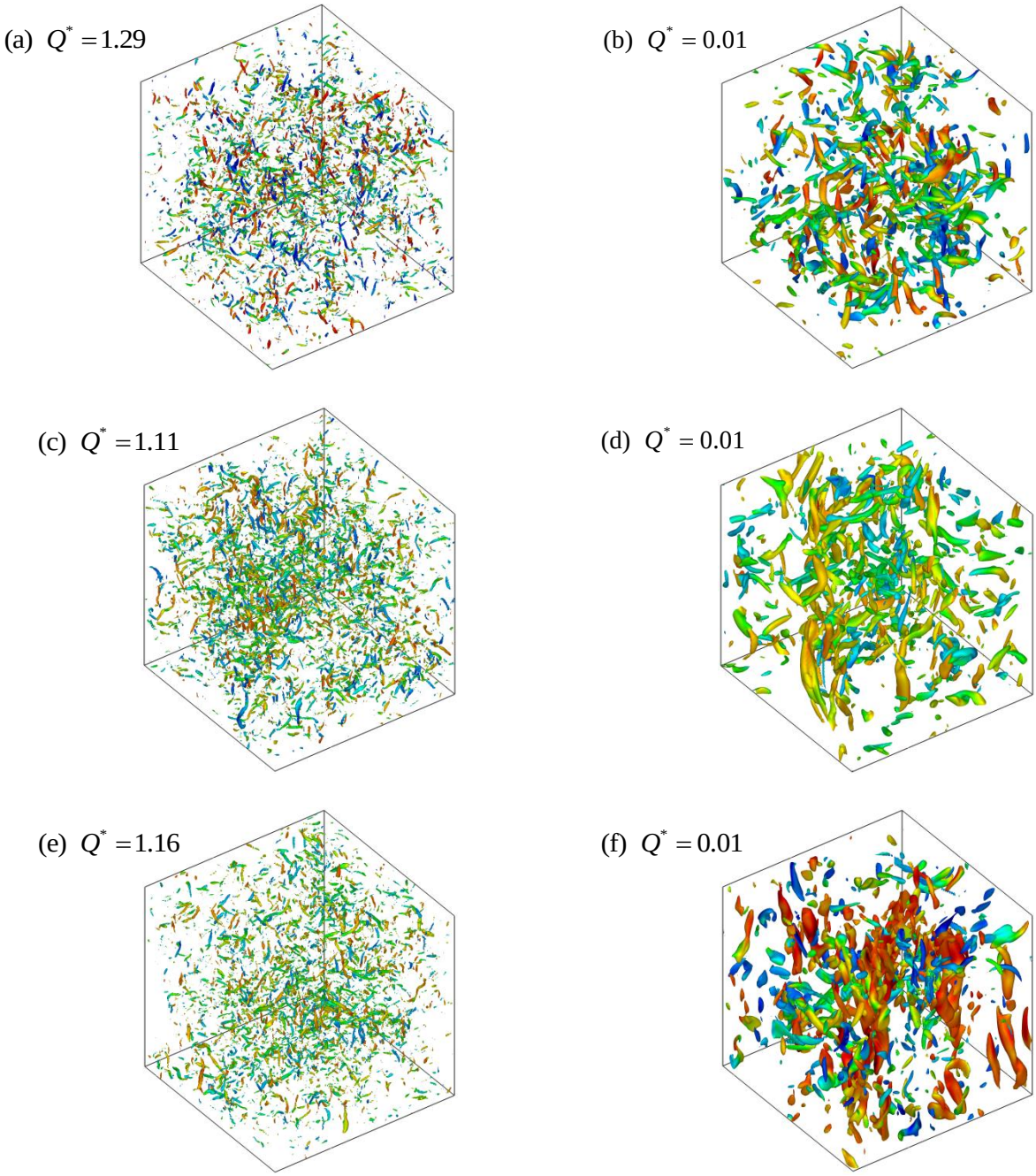

Figure 2. Isosurface of the second invariant of the velocity gradient tensor (Q^*), coloured by the vertical vorticity, at (left) $t^* = 1.7$ and (right) $t^* = 8.5$ for (a, b) $N = 0$, (c, d) $N = 0.25$ and (e, f) $N = 0.5$.

number. For the case of $N = 0$, the Taylor's microscale is about 0.33 and increases to 0.4 and 0.46 once the rotation number increases to 0.25 and 0.5, respectively. For a very low angular velocity ($N = 0.25$), the turbulence structures are still isotropic. The anisotropic of the turbulence structures seems to appear when the rotation number is about 0.5. This leads to the appearance of the columnar vortices, as illustrated in figure 2(f). Thus, it can be concluded that at the early time ($t^* = 0 - 8.5$) the

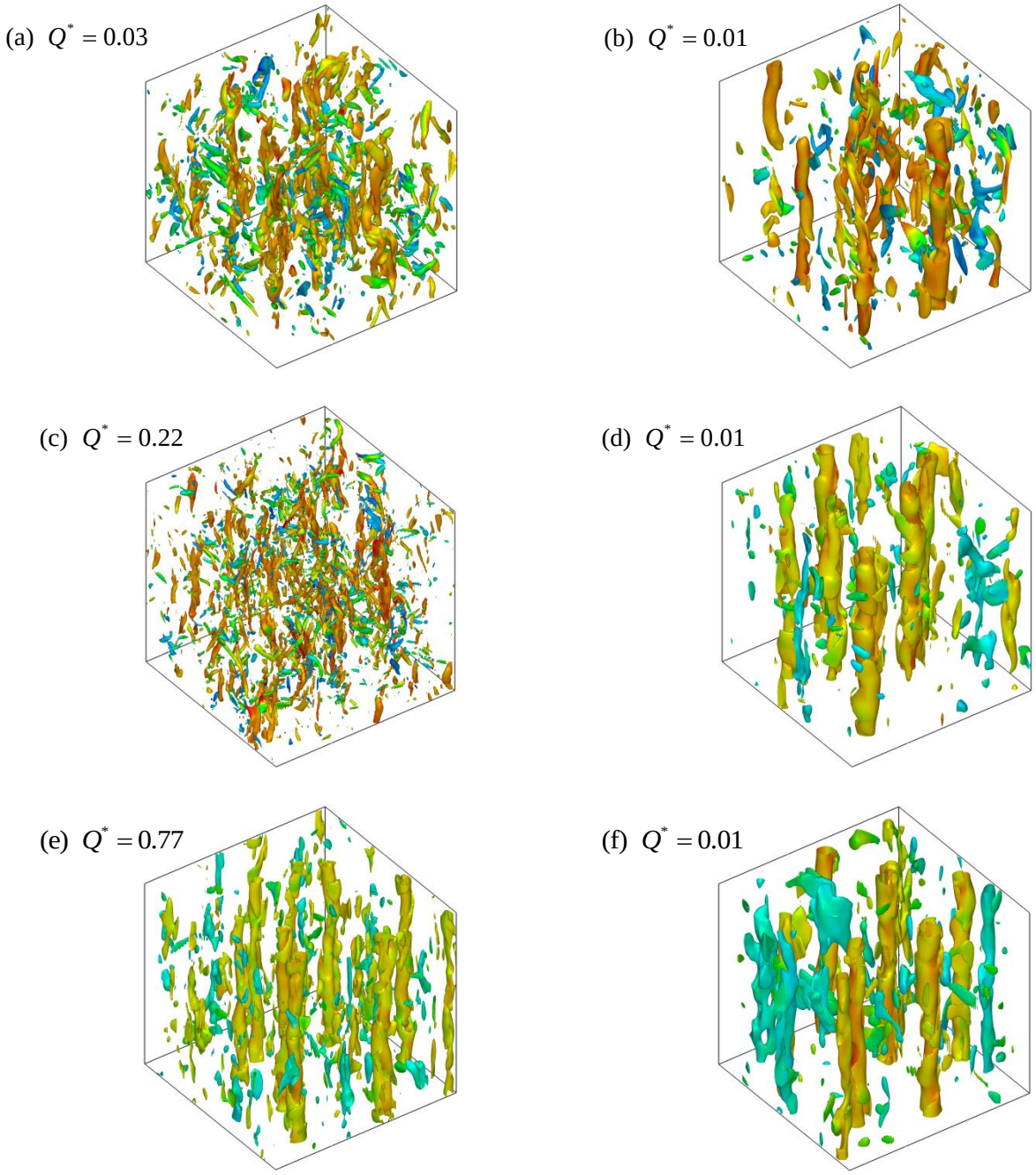

Figure 3. Isosurface of the second invariant of the velocity gradient tensor (Q^*), coloured by the vertical vorticity, at (a, b) $N = 1; t^* = 4.7, 8.5$, (c, d) $N = 2; t^* = 2.7, 8.5$ and (e, f) $N = 4; t^* = 1.2, 8.5$ respectively.

turbulence structures are not influenced much when a frame of reference rotates slowly ($N < 0.5$). For strong background rotation cases ($N = 1$, 2 and 4), the turbulence structures develop in a different way and look more anisotropic, as shown in figures 3(a), 3(c) and 3(e). Additionally, the formation of the columnar vortices seems to form very quickly. It should be noted that the time that the columnar vortices appear depends strongly on the rotation number. They form earlier with an increase in the

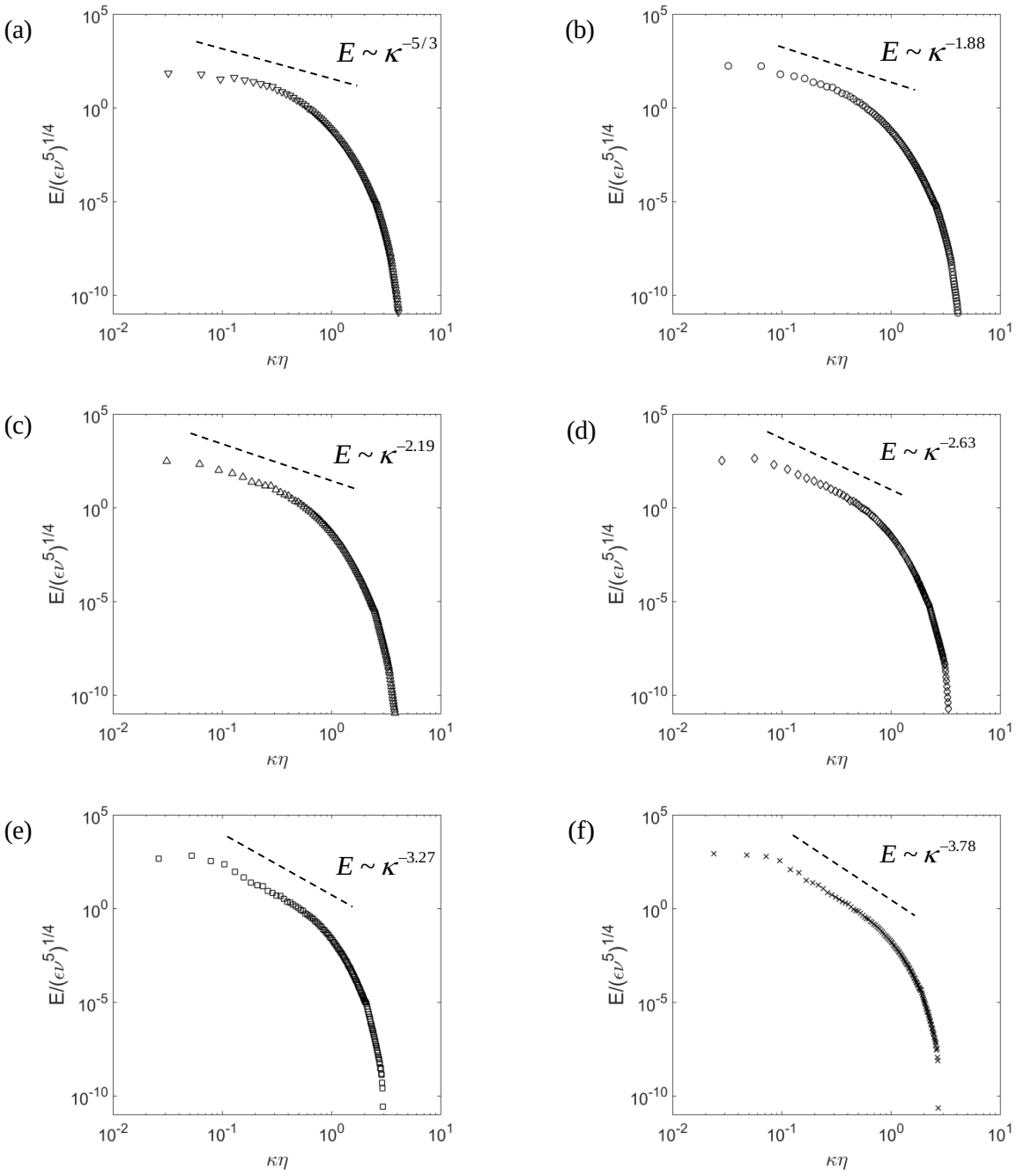

Figure 4. The energy spectrum normalised in Kolmogorov variables at $t^* = 8.5$ of; (a) $N = 0$, (b) $N = 0.25$, (c) $N = 0.5$, (d) $N = 1$, (e) $N = 2$ and (f) $N = 4$.

rotation rate. With time, the small-scale structures are merged with each other, resulting in the formation of quantitatively large vertical vortex. These large-scale coherent structures are stretched in the vertical direction, leading to the appearance of the columnar vortices.

At $t^* = 8.5$, the length of the columnar vortices increases with an increase in the external rotation rate ($\lambda = 0.45$, 0.47 and 0.51 for $N = 1$, 2 and 4), while their number reduces. This suggests that the fast background rotation rate quickly alters the isotropic behaviour of the turbulence structures, yielding the occurrence of the columnar vortices.

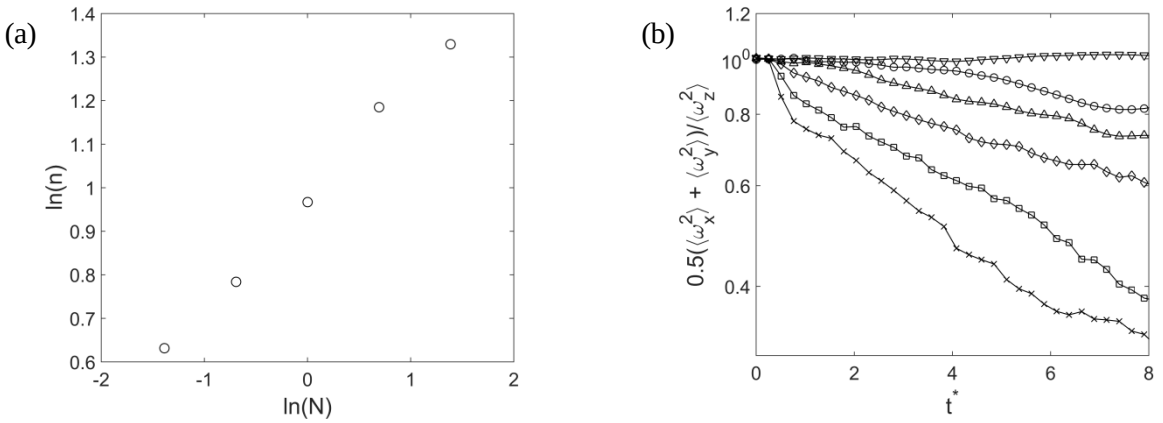

Figure 5. (a) The Slopes of each case on figure 6 and (b) The history of integral of $0.5\left(\left\langle\omega_x^2\right\rangle+\left\langle\omega_y^2\right\rangle\right)/\left\langle\omega_z^2\right\rangle$ for ▽ $N=0$, ○ $N=0.25$, △ $N=0.5$, ◊ $N=1$, □ $N=2$ and × $N=4$.

3.2. *Spectral Analysis*

The changes from isotropic to anisotropic behaviour of the turbulent structures can be observed by the plot of the three-dimensional energy spectrum, normalised by Kolmogorov variables, written as

$$E(\kappa,t)=\int_0^\infty\int_0^\infty\int_0^\infty\frac{1}{2}\left|\hat{u}_i(\kappa,t)\right|^2 d\kappa_x d\kappa_y d\kappa_z \tag{6}$$

where ε is dissipation rate and η is Kolmogorov length scale. Figure 4 illustrates the normalised energy spectrum for all cases at $t^*=8.5$. For $N=0$, the energy spectrum in the inertial subrange exhibits a slope $E\sim\kappa^{-5/3}$ [18], as shown in figure 4(a). When the frame of reference rotates in the vertical direction (figures 4b – 4f), the energy spectrum decays very quickly. The slopes are dropped to $E\sim\kappa^{-3.78}$ for the case of $N=4$. The range of inertial subrange seems to increase with an increase in the rotation number. This leads to the occurrence of an inverse energy cascade (recalled that the energy is usually transferred from low-wave numbers to high-wave numbers for normal turbulence, in contrast when an inverse energy cascade occurs, the energy is transferred from high-wave numbers to low-wave numbers).

Figure 5(a) shows the slope (n) of the energy spectrum in the inertial subrange of each case. The slope increases with the rotation number as $n\sim N^{0.26}$. The time history of the ratio of the lateral component of the volume-integrated vorticity to its vertical component $0.5\left(\left\langle\omega_x^2\right\rangle+\left\langle\omega_y^2\right\rangle\right)/\left\langle\omega_z^2\right\rangle$ is illustrated in figure 5(b). For zero and low rotation numbers ($N=0$, 0.25 and 0.5) the turbulence structures are also isotropic at the early time ($t^*=1.7$) due to the fact that $\langle\omega_x\rangle\approx\langle\omega_y\rangle\approx\langle\omega_z\rangle$. On the other hands, for moderate and strong rotation numbers ($N=1$, 2 and 4), the vertical vorticity ω_z is greater than the lateral components, suggesting that the turbulence structures are anisotropic. This is confirmed by the flow visualisation displayed in figure 3. With time, the effect of the external rotation is more influenced, resulting in $\langle\omega_z\rangle>>\langle\omega_x\rangle,\langle\omega_y\rangle$. The anisotropy of the turbulence structures becomes stronger with increasing rotation number.

4. Conclusion

Direct numerical simulation is used to investigate the effect of background rotation on the evolution of homogeneous isotropic turbulence. The rotation number is varied from $N = 0$ to 4. At low rotation numbers ($N = 0.25$ and 0.5), the turbulence structures does not feel an effect of the background rotation much and develops as isotropic turbulence at early time. With time, the background rotation plays a role in changing the isotropic behaviour of the turbulence structures. For fast rotation rates ($N = 1$, 2 and 4), the anisotropy of the turbulence structures develops very quickly. This leads to the appearance of the large-scale vertical vortices. An inverse energy cascade seems to appear in the inertial subrange once the background rotation is active. The slope of the energy spectrum in the inertial subrange increases with the rotation number as $n \sim N^{0.26}$.

Acknowledgement

The authors gratefully acknowledge the financial support from Chiang Mai University and the use of HPC services of the Faculty of Engineering, Chiang Mai University.

References

[1] Morize C, Moisy F and Rabaud M 2005 *Physics of Fluids* **17**
[2] Bardina J, Ferziger J H and Rogallo R S 1985 *J. of Fluid Mechanics* **154**
[3] Mansour N N, Cambon C and Speziale C G 1992 *Theoretical and computational study of rotating isotropic turbulence Studies in Turbulence* (New York: Springer)
[4] Hossain M 1994 *Physics of Fluids* **6**
[5] Godeferd F S and Lollini L 1999 *Journal of Fluid Mechanics* **393**
[6] Morinishi Y, Nakabayashi K and Ren S Q 2001 *Physics of Fluids* **13**
[7] Hopfinger E J, Browand F K and Gagne Y 1982 *J. of Fluid Mechanics* **125**
[8] Yeung P K and Zhou Y 1998 *Physics of Fluids* **10**
[9] Thiele M and Müller W C 2009 Structure and decay of rotating homogeneous turbulence *J. of Fluid Mechanics* **637**
[10] Smith L M and Waleffe F 1999 *Physics of Fluids* **11**
[11] Mininni P D, Alexakis A and Pouquet A 2009 *Physics of Fluids* **21**
[12] Baqui Y B and Davidson P A 2015 *Physics of Fluids* **27**
[13] Yang X and Domaradzki J A 2004 Large eddy simulations of decaying rotating turbulence *Physics of Fluids* **16**
[14] Rogallo R S 1981 *NASA Technical Memorandum*
[15] Spalart P E, Moser R D and Rogers M M 1991 *J. of Computational Physics* **96**
[16] Orlandi P 2000 *Fluid Flow Phenomena a Numerical Toolkit* (Rome: Springer)
[17] Mansour N N and Wray A A 1994 *Physics of Fluids* **6**
[18] Smith L M and Reynolds W C 1991 *Phys. Fluids A* **3**